Regular Article

Gravitational compression of colloidal gels

J.J. Liétor-Santos[a], C. Kim[b], P.J. Lu, A. Fernández-Nieves[a,c], and D.A. Weitz

Department of Physics and HSEAS, Harvard University, Pierce Hall, 29 Oxford street, Cambridge, MA, 02138, USA

Abstract. We study the compression of depletion gels under the influence of a gravitational stress by monitoring the time evolution of the gel interface and the local volume fraction, ϕ, inside the gel. We find ϕ is not constant throughout the gel. Instead, there is a volume fraction gradient that develops and grows along the gel height as the compression process proceeds. Our results are correctly described by a non-linear poroelastic model that explicitly incorporates the ϕ-dependence of the gravitational, elastic and viscous stresses acting on the gel.

PACS. 82.70.Gg Gels and sols – 47.56.+r Flows through porous media – 82.70.Dd Colloids

1 Introduction

In the presence of attractive interactions, colloidal systems can form gels, which are kinetically arrested particle-networks that span the space provided by the container. Physically, gelation is related to an arrested spinodal decomposition process, where colloid-rich and colloid-poor regions become kinetically trapped preventing the complete phase separation of the system [1,2]. The required attraction between particles is often provided by adding non-adsorbing polymer to a stable dispersion of particles to induce a depletion interaction between them. In this case, when two particles come close enough, there is a reduction in the excluded volume, V, where polymer chains cannot penetrate, and an unbalanced osmotic pressure, Π; the result is an attraction between particles with a magnitude $U \approx \Pi V$ and a range that is determined by the polymer size [3].

Formation of a network changes the mechanical properties of the system; gels are elastic at low frequencies and thus can support stress. However, the presence of a gravitational stress can cause the slow compression of the structure and result in an elastic deformation of the gel. Eventually, however, the compression process stops; this steady state is reached when the elastic and gravitational stresses are balanced everywhere in the gel. The overall compressive behavior has been described using a linearized poroelastic model [4]. Within this model, the gravitational

stress is everywhere balanced by the sum of a frictional stress, which results from the fluid flow through the particle network, and the elastic stress of the gel. Interestingly, at the end of the compression process, in the steady state, the volume fraction, ϕ, is not constant and exhibits a height dependence [5]: Since the gravitational stress increases in the settling direction, the elastic stress cannot be uniform throughout the gel causing the observed volume fraction gradient along its height. This behavior is also correctly described by a non-linear poroelastic model that describes this ϕ-dependence and that also predicts how it should continually evolve in time as the compression of the gel proceeds. This time evolution, however, has never been measured experimentally.

In this paper, we present measurements of the compression of depletion gels in the presence of gravitational stresses. The particle volume fraction as a function of height at any time is measured with a non-invasive method by monitoring the intensity of transmitted light through the sample. We compare the experimental data to the predictions of the extended poroelastic model for the time evolution of the gel interface and the dependence of particle volume fraction with height and time. We find that the agreement between our results and the theoretical predictions is very good.

2 Experimental set-up

We use polymethylmethacrylate (PMMA) particles (University of Edinburgh) [6], with radius $a = (2.0 \pm 0.2)\,\mu$m stabilized by a layer of polyhydrostearic acid (PHSA) in a $5:1$ mixture by volume of bromocyclohexane and decahydronaphtalene which closely matches the index of refraction of the particles. The PMMA particles are labeled with

---

[a] *Present address:* School of Physics, Georgia Institute of Technology, 837 State street, Atlanta, GA 30332-0430, USA.

[b] *Present address:* Chemical Physics Interdisciplinary Program, Liquid Crystal Institute, Kent State University, Kent, OH 44242, USA.

[c] e-mail: `alberto.fernandez@physics.gatech.edu`
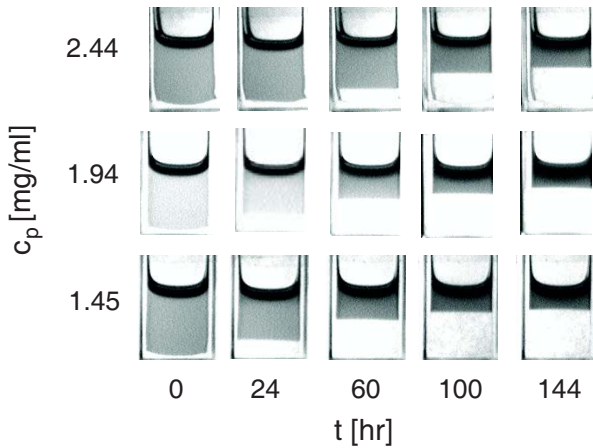
Fig. 1. (Color online) Snapshots at different stages during the compression of various colloidal gels with $\phi_0 = 0.08$ and different polymer concentrations.

Nile Red dye [7,8]. In order to induce an attraction between particles, we add non-adsorbing linear polystyrene (Polymer Labs) of molecular weight $M_w \approx 1.3 \cdot 10^7$ g/mol, and polydispersity index $\frac{M_w}{M_n} \approx 1.03$, where M_n is the number average molecular weight. Using static light scattering, we find that the radius of gyration of the polymer under very dilute conditions, $c \to 0$, is $r_g \approx 150$ nm, and the overlap concentration is $c^* = 0.6$ mg/ml. To screen possible electrostatic interactions between particles [9], we add 8 mM of the salt tetrabutylammonium chloride (TBAC); this results in a Debye screening length of 8 nm [10].

All samples have the same initial volume fraction, $\phi_0 \approx 0.08$, and different polymer concentrations ranging from 1.45 mg/ml to 2.44 mg/ml. In all cases, we confirmed the formation of gels by looking at the samples using confocal microscopy. Experiments are performed in 1 cm square glass cuvettes filled up to a height $h_0 = 1$ cm and sealed to prevent evaporation. The solvent mixture matches the density of the particles at room temperature as well as the refractive index of the particles. We induce a controlled density mismatch, $\Delta\rho$, by setting a constant temperature of 5 °C; since the thermal expansion coefficient of the organic solvents, which is around $10^{-3}/°$C [11], is higher than that of PMMA, which is around $\approx 2.5 \cdot 10^{-4}/°$C [12], a density difference of $\Delta\rho \approx -50$ kg/m^3 is induced at this temperature. After vigorously shaking the samples for 1 minute, we monitor the settling behavior of the gel using a charge-coupled device (CCD) camera. The cells are illuminated from behind with a lamp that provides acceptable uniformity in light intensity.

3 Results and discussion

The snapshots in Figure 1 are representative examples of the compression process at different times for three different polymer concentrations. All samples cream and eventually reach a steady-state regime characterized by the absence of compression; the time scale associated to the
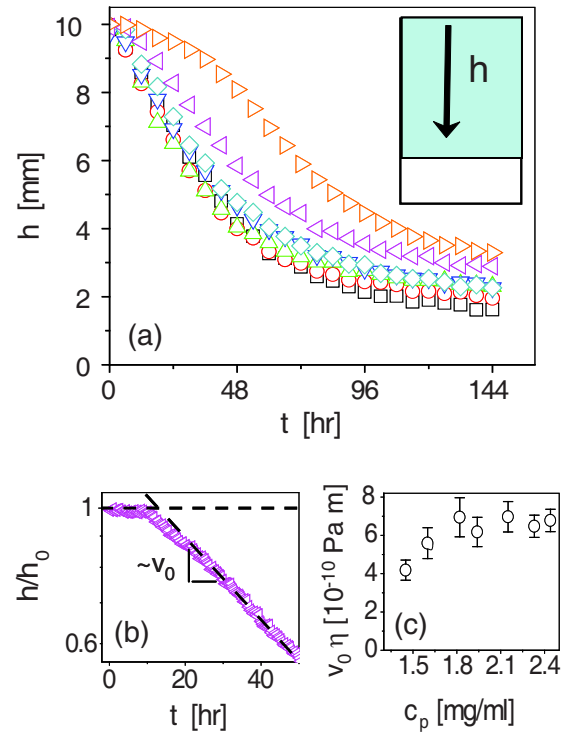
Fig. 2. (Color online) (a) Interface height, h, as a function of time, for different polymer concentrations. □: 1.45 mg/ml; ○: 1.60 mg/ml; △: 1.82 mg/ml; ▽: 1.94 mg/ml; ◇: 2.15 mg/ml; ◁: 2.33 mg/ml; ▷: 2.44 mg/ml. h is measured from the top of the gel, as shown in the schematic. (b) Blow-up of the initial compression stage for the 2.33 mg/ml sample. (c) Re-scaled velocity, obtained by multiplying the initial velocity of the gel and the solution viscosity, as a function of polymer concentration.

whole process is about one week. To quantify the time evolution of the gel, we analyze the images near the center of the cells and identify the gel interface separating the dark upper phase, corresponding to the creaming gel, and the brighter lower phase, corresponding to the solvent. We find that the height of this interface, h, measured from the top of the cell, decreases with time as the compression proceeds, as shown in Figure 2(a). This happens for all polymer concentrations.

In the initial stages of the process, however, we observe that there is a delay time, t_d, below which the interface does not move. We estimate t_d from the crossover between the horizontal and the initial slope of the creaming process, as shown in Figure 2(b). This time is constant for small c_p and increases with polymer concentration for the highest c_p, as shown in Figure 3. We believe depletion interactions between the particles and the bottom wall of the cell are likely responsible for this behavior [13]. However, this corresponds to only a small fraction of the total compression time and we do not consider it in any further analysis. After this initial time, the gels start to cream. From the initial stages of the process we can determine the initial creaming speed, v_0, which we obtain from the slope of a linear fit of the first points of the interface evolution [4], as shown in Figure 2(b). We find that this
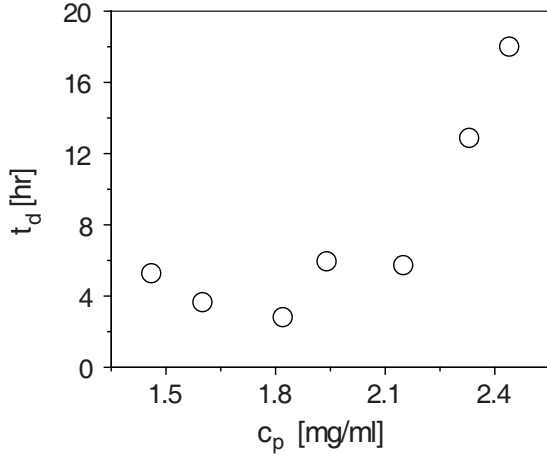
Fig. 3. Delay times obtained from the experimental height profiles as a function of polymer concentration.

Fig. 4. Calibration of the grayscale intensity and the particle volume fraction, ϕ. The solid line is the best fit to a logarithmic function (see text), with $A_1 = 0.9 \pm 0.2$ and $A_2 = 271 \pm 5$.

initial speed decreases with increasing polymer concentration. This essentially results from the viscosity increase with c_p, as shown in Figure 2(c), where we plot a re-scaled velocity, obtained by multiplying the initial speed of the compression and the solution viscosity, η, as a function of polymer concentration; we find that $v_0 \eta$ is essentially constant throughout our polymer concentration range.

In the latest stages of the creaming process, the system reaches a steady-state regime characterized by the absence of compression. As a result, the interface height remains constant with time. It, however, increases with polymer concentration, as can be seen from the long-time behavior of h in Figure 2(a). This reflects the balance between the elastic stress, σ_e, in the network and the gravitational stress, σ_g; the viscous stress does not contribute to the stress balance in this case since there is no motion of the gel nor of the solvent. Thus, for $t \to \infty$
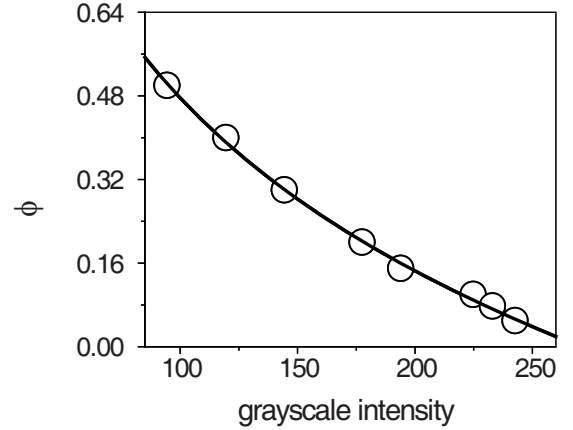
$$d\sigma_e = -\frac{K(\phi_\infty)}{\phi_\infty(z)} d\phi_\infty(z) = \Delta\rho g \phi_\infty(z) dz = d\sigma_g, \quad (1)$$

where we have used the definition of the compressional modulus, $K = -\phi \frac{\partial \sigma_e}{\partial \phi}$ [14], which is the relevant modulus in our problem. Here, $\phi_\infty(z)$ is the volume fraction in the steady state at a distance z from the top of the gel. Since the elastic stress depends on the volume fraction as [5]

$$\sigma_e(z,t) = \alpha \frac{\phi(z,t) - \phi_g}{\phi_{rcp} - \phi(z,t)}, \quad (2)$$

with α a stiffness parameter accounting for the particle-particle interaction, $\phi_{rcp} = 0.64$ and $\phi_g \approx 0.03$ the minimum volume fraction to have a gel [8,15], we can integrate equation (1) to obtain the volume fraction profile in the steady state as a function of z

$$\frac{\phi_{rcp}(\phi_\infty(z) - \phi_0)}{(\phi_{rcp} - \phi_\infty(z))(\phi_{rcp} - \phi_0)}$$
$$+ \ln \frac{\phi_\infty(z)(\phi_{rcp} - \phi_0)}{\phi_0(\phi_{rcp} - \phi_\infty(z))} = \frac{\Delta\rho g (z - h_f)\phi_{rcp}^2}{\alpha(\phi_{rcp} - \phi_g)}, \quad (3)$$

where h_f is the final height of the experiment, which depends on the polymer concentration.

We measure the volume fraction profiles from the grayscale intensity, I, of the optical images taken during the compression process [16,17]. For this purpose, we perform an intensity-concentration calibration and adjust the illumination intensity to maximize the range of grayscale intensity and prevent saturation of the CCD camera. We measure I from samples of known volume fraction, which we vary within a range of 5–50%. The results indicate that I increases with decreasing ϕ, as shown in Figure 4. The calibration can be fitted with a logarithmic function of the form

$$\phi = A_1 \log\left(\frac{A_2}{I}\right), \quad (4)$$

where A_1 and A_2 are two fitting parameters accounting for sample properties and incident light intensity, respectively. From the experimental calibration, we obtain $A_1 = 0.9 \pm 0.2$ and $A_2 = 271 \pm 5$. In general, these parameters will depend on the choice of light illumination; this would require their determination for each experimental cell, since there could be slight differences in sample illumination among them. Instead, we calculate A_1 and A_2 for each cell using two boundary conditions: i) the initial intensity at $t = 0$, I_0, which corresponds to the initial volume fraction, ϕ_0, and ii) mass conservation, which must be fulfilled at any time during the compression process. Since the mass of all particles in the compressed gel, $\int_0^{h(t)} \phi(z)dz$, should be equal to the total mass in the initial state, $\phi_0 h_0$, this condition can be expressed as $\int_0^{h(t)} \phi(z)dz = \phi_0 h_0$. We obtain

$$A_1 = \frac{\phi_0[h_0 - h(t)]}{h(t)\log I_0 - B}, \quad (5)$$

$$A_2 = 10^{\frac{\phi_0}{A_1}} I_0, \quad (6)$$

where I_0 is measured from the initial image and $B = \int_0^{h(t)} \log I\, dz$ is determined from the images at any intermediate time, t; we checked that the particular choice of
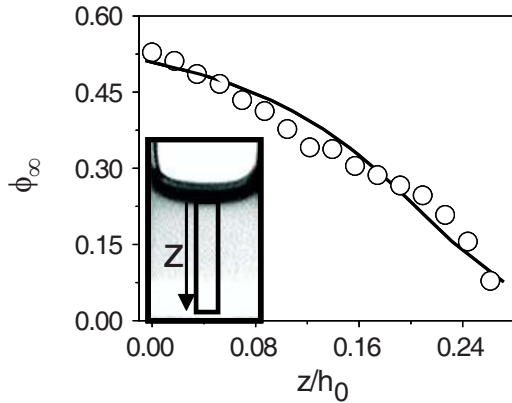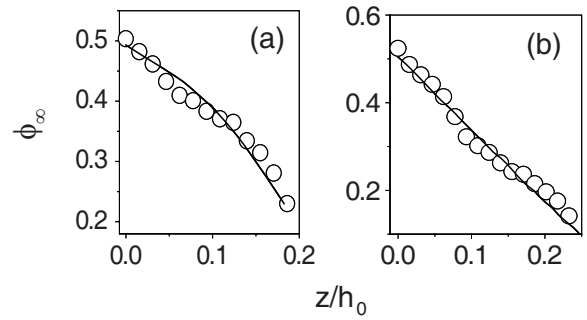
Fig. 5. Dependence of the volume fraction with a normalized distance from the sample top in the steady state. $c_p = 2.15\,\mathrm{mg/ml}$. The line shows the best fit based on the predictions of the poroelastic model (see text). The only fitting parameter is α. We obtain $\alpha \approx 0.1\,\mathrm{Pa}$. Inset: image at $t = 25\,\mathrm{h}$. The rectangle shows the slice we consider to obtain the intensity grayscale variation with height in the experiment. For a given height, we average over the width of this rectangle. The data points have a 10% error corresponding to the standard deviation of three independent experiments.


Fig. 6. Dependence of the volume fraction with the normalized distance from the sample top in the steady state. (a) $c_p = 1.82\,\mathrm{mg/ml}$, (b) $c_p = 2.33\,\mathrm{mg/ml}$. The lines represent the best fit to the poroelastic model predictions, with α as fitting parameter. We find $\alpha \approx 0.07\,\mathrm{Pa}$ for $c_p = 1.82\,\mathrm{mg/ml}$ and $\alpha \approx 0.14\,\mathrm{Pa}$ for $c_p = 2.33\,\mathrm{mg/ml}$.


Fig. 7. (Color online) Linear dependence of α with the attractive force, U/r_g, per unit area, πa^2. Our experimental points are represented by circles (with their error bars), while the squares correspond to the experimental results of Kim *et al.* [5].

time for the calculation does not alter the values of A_1 and A_2, as expected, since illumination within one cell does not change with time. We confirm the validity of our approach by performing an experiment with a sample at a polymer concentration $c_p = 1.9\,\mathrm{mg/ml}$ under the illumination conditions of the calibration. We obtain $A_1 = 0.98$ and $A_2 = 278$ from equation (5) and equation (6), which are in a very good agreement with the values obtained experimentally for the calibration.

Using equation (4) and the boundary conditions to calculate A_1 and A_2, we obtain the volume fraction profiles, $\phi_\infty = \phi_\infty(z)$, for a gel formed at $c_p = 2.15$ mg/ml. We observe that $\phi_\infty(z)$ decreases with increasing z, as shown in Figure 5; similar results are obtained for other polymer concentrations, as shown in Figure 6. We also find that ϕ is equal to ϕ_0 at the bottom of the gel and close to 0.5 at the top; the upper part of the gel supports the weight of the remaining structure causing a rearrangement in the particle concentration within the network to increase ϕ up to the observed values. We can fit the experimental volume fraction profiles using equation (3), leaving α as the only fitting parameter. We find that the prediction of the poroelastic model for the long-time volume fraction profile is consistent with our observations, with $\alpha \sim 0.1\,\mathrm{Pa}$.

Based on equation (2) for the elastic stress and on its balance with the gravitational stress in the steady state, the value of α must be of the order of σ_g. In the experiment of Figure 5, $\sigma_g = 0.4\,\mathrm{Pa}$, which is of the order of the value of α obtained from the fit. The stiffness parameter modulates the $(\phi_{rcp} - \phi)^{-1}$ dependence of the elastic stress; it accounts for the attractive interactions between particles that ultimately induce gelation and provide strength to the gel [5]. Since it has units of stress, it must scale with the force between particles, which we take as the energy
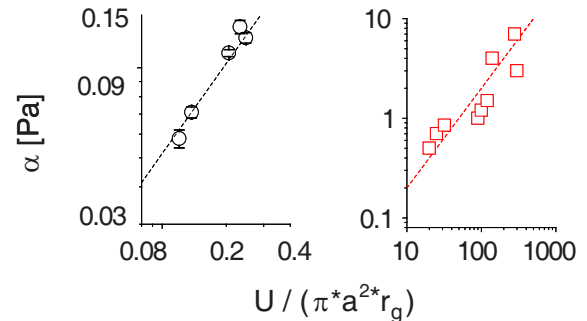
over the width of a particle-particle bond, U/r_g, divided by a cross-sectional area, a^2. Thus, $\alpha \sim U/(r_g a^2)$. This scaling is confirmed by our experimental results, as shown by the circles in Figure 7. In this same figure, we also show with squares the experimental values of α for a system of emulsions and either polymer or micelles as depletants [5]. In this case also, α depends linearly on $U/(r_g a^2)$ and is of the order of the gravitational stresses applied to induce the creaming of the emulsion gel.

During the compression of the structure, fluid is expelled through the pores of the gel. The fluid flow associated to this process can be related to the pressure gradient along the gel by means of Darcy's law [18]

$$v = -\frac{\kappa(\phi)}{\eta}\frac{\partial p}{\partial z}, \qquad (7)$$

where v is the velocity of the interface, p is the fluid pressure, and $\kappa(\phi) = \kappa_0 \left[\frac{\phi_0}{\phi(z,t)}\right]^{\frac{2}{3-d_f}}$ is the permeability of the network [4], with κ_0 its permeability in the initial compression stages, when $\phi = \phi_0$, and d_f its fractal dimension. Using confocal microscopy, we estimate that $d_f \approx 2$ for our gels [19].
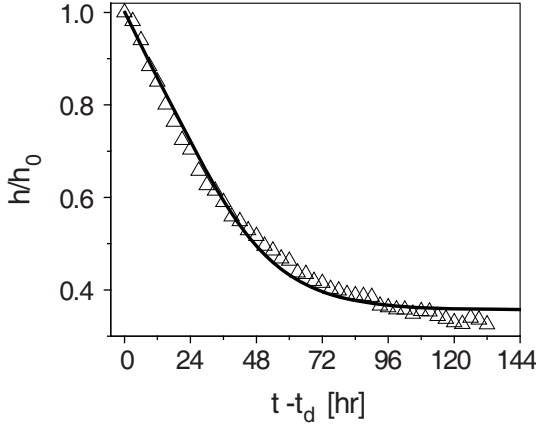
Fig. 8. Comparison between the measured time evolution of the normalized gel interface (points) and the calculations based on the poroelastic model (line) for $c_p = 2.15$ mg/ml.

The frictional stress between the gel and the background solvent is given by

$$\sigma_v(z) = \int_{h(t)}^{z} \gamma v \mathrm{d}z' = -\int_{h(t)}^{z} \frac{\partial p}{\partial z'} \mathrm{d}z', \qquad (8)$$

where we have used Darcy's law and $\gamma = \frac{\eta}{\kappa(\phi)}$ is the friction coefficient per unit of volume.

At any time, the evolution of the interface is governed by the balance between the gravitational stress gradient and the elastic and frictional stress gradients in the gel [4]

$$\Delta\rho g\phi(z,t) = \frac{\partial p}{\partial z} + \frac{K(\phi)}{\phi(z,t)}\frac{\partial\phi(z,t)}{\partial z}. \qquad (9)$$

In addition, mass conservation must be fulfilled

$$\frac{\partial\phi(z,t)}{\partial t} + \frac{\partial}{\partial z}(\phi(z,t)v) = 0. \qquad (10)$$

Combining equations (9) and (10), we obtain the following equation:

$$\frac{\partial p}{\partial t} - \frac{K(\phi)}{\phi(z,t)}\frac{\partial}{\partial z}\left(\frac{\phi(z,t)\kappa(\phi)}{\eta}\frac{\partial p}{\partial z}\right) - \frac{\Delta\rho g\phi(z,t)\kappa(\phi)}{\eta}\frac{\partial p}{\partial z} = 0, \qquad (11)$$

which we can solve numerically together with equation (10) to obtain $\phi(z)$ at any given time. Once the volume fraction height dependence is known for that time, we can determine the interface position, $h(t)$, by considering that all mass lies in the gel region and thus $\int_0^{h(t)}\phi(z,t)\mathrm{d}z = \phi_0 h_0$. A comparison between the experimental results and the theoretical predictions, for $c_p = 2.15$ mg/ml, is shown in Figure 8. In the experiment, we do not consider the initial delay time and thus present the results in terms of a relative time scale, $t-t_d$. The solid line is a fit to the poroelastic model, with α and κ_0 left as fitting parameters; we obtain $\alpha = 0.21$ Pa and $\kappa_0 = 7.25 \cdot 10^{-11}$ m^2, which agree with the steady-state result obtained for the stiffness parameter and with the
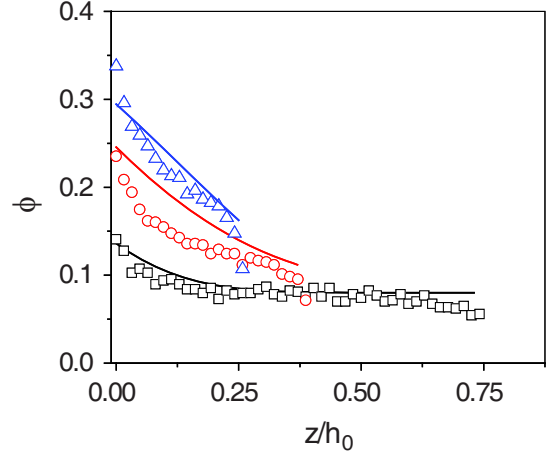
Fig. 9. (Color online) Dependence of the volume fraction with the normalized distance from the cell top for $t = 24$ h (black squares), $t = 60$ h (red circles) and (d) $t = 100$ h (blue triangles). $c_p = 2.15$ mg/ml. The lines correspond to the predictions of the poroelastic model without fitting parameters.
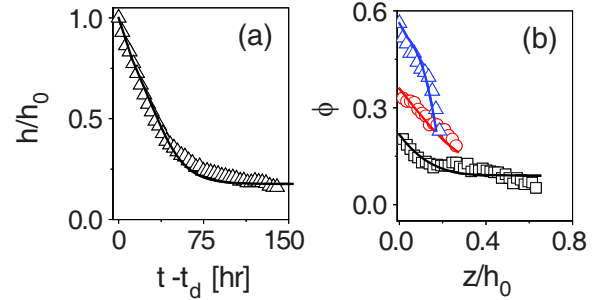
Fig. 10. (Color online) Comparison between experimental results and poroelastic model predictions for $c_p = 1.60$ mg/ml. (a) Normalized interface height *versus* the re-scaled time, $t-t_d$. (b) Volume fraction *versus* normalized distance measured from the gel top, for $t = 30$ h (black squares), $t = 100$ h (red circles) and for the steady state (blue triangles).

permeability derived from the initial slope of the creaming profiles, $\kappa_0 = (7.7 \pm 0.1) \cdot 10^{-11}$ m^2 [20].

The time dependence of $\phi(z,t)$ also agrees with the experimental data, as shown in Figure 9. In this case, there are no fitting parameters; we use the independently obtained parameters that correctly describe the interface evolution.

As an additional example of our typical results, we also present in Figure 10 the experimental interface height and volume fraction profile for $c_p = 1.6$ mg/ml, together with the theoretical predictions of the poroelastic model. From the fit of the gel interface to the theory, we obtain $\alpha \approx 0.07$ Pa and $\kappa_0 = 6.8 \cdot 10^{-11}$ m^2, which is in reasonable agreement with the permeability value obtained from the initial compression stages, $\kappa_0 = (5.7 \pm 0.1) \cdot 10^{-11}$ m^2.

Finally, we note that there is a noticeable change in the curvature of the $\phi(z)$ profiles as time proceeds. While at the beginning of the compression process the shape of $\phi(z)$ is concave, at later times, $\phi(z)$ has become convex.

This change in shape results from the migration of particle from the bottom of the gel towards its top, where the gravitational stress is larger. During the first compression stages, some particles move to the top part of the gel in order to support the weight of the whole column of material lying below. As time proceeds, however, it is increasingly more difficult to place particles at the top part of the gel, and the intermediate regions start to get filled with particles. The result is the shape change observed in Figures 9 and 10(b).

4 Conclusion

We have shown that the compression of a gel under gravitational stress induces a particle volume fraction gradient along the gel height, which evolves continuously until steady-state conditions are reached. The experiments allow the determination of this gradient *in situ* without perturbing the compression evolution. Our results are in very good agreement with a non-linear poroelastic model that explicitly accounts for the height dependence of the volume fraction. We show that this model correctly describes the gel height evolution, the steady-state volume fraction profile and its time dependence, highlighting the generality of the theory to accurately describe the compression of gels.

References

1. G. Foffi, C.D. Michele, F. Sciortino, P. Tartaglia, Phys. Rev. Lett. **94**, 078301 (2005).
2. N.A.M. Verhaegh, D. Asnaghi, H.N.W. Lerkkerkerker, M. Giglio, L. Cipelletti, Physica A **242**, 104 (1997).
3. S. Asakura, F. Oosawa, J. Chem. Phys. **22**, 1255 (1954).
4. S. Manley, J.M. Skotheim, L. Mahadevan, D.A. Weitz, Phys. Rev. Lett. **94**, 218302 (2005).
5. C. Kim, Y. Liu, A. Kühnle, S. Hess, S. Viereck, T. Danner, L. Mahadevan, D.A. Weitz, Phys. Rev. Lett. **99**, 028303 (2007).
6. L. Antl, J. Goodwin, R. Hill, S. Owens, S. Papworth, J.A. Waters, Colloid Surf. **17**, 67 (1986).
7. P. Greenspan, E. Mayer, S. Fowler, J. Cell. Biol. **100**, 965 (1985).
8. P.J. Lu, J.C. Conrad, H.M. Wyss, A.B. Schofield, D.A. Weitz, Phys. Rev. Lett. **96**, 028306 (2006).
9. A. Yethiraj, A. Blaaderen, Nature (London) **421**, 513 (2003).
10. M.F. Hsu, E.R. Dufresne, D.A. Weitz, Langmuir **21**, 4881 (2005).
11. D.R. Lide, *79th CRC Handbook of Chemistry and Physics* (CRC Press, Boca Raton, 1999).
12. J. Brandup, *Polymer Handbook* (Wiley, New York, 1998).
13. We have performed similar experiments with polystyrene particles in the presence of non-adsorbing polymer. In this case, the system does not cream but rather sediments along the gravitational direction; as a result there are no depletion interactions with the upper liquid-air interface. Consistent with this, we find no delay time.
14. R. Buscall, Colloid Surf. **5**, 269 (1982).
15. The volume fraction for gelation is taken from [8], which contains the phase diagram for our experimental system.
16. The length scale of a pixel in one of our images is $10\,\mu$m. We thus expect that the structure of the colloidal suspension should not greatly affect the transmission through the sample. We also assume that contributions arising from the scattering from other parts of the cell are negligible compared to the transmission [17].
17. J.K.G. Dhont, *An Introduction to the Dynamics of Colloids* (Elsevier, Amsterdam, 1996).
18. H. Darcy, *Les fontaines publiques de la ville de Dijon* (Dalmont, Paris, 1856).
19. A.D. Dinsmore, V. Prasad, I. Wong, D.A. Weitz, Phys. Rev. Lett. **96**, 185502 (2007).
20. In the initial compression stages, the gel does not change appreciably its volume fraction. As a result, the elastic stress gradient in equation (9) can be neglected. The initial stages are thus determined by the balance between the gravitational and frictional stress gradients. This is used to determine the initial permeability of the gel from the slope of the interface evolution with time. See [4] for further details.